Journal of
Mechanics of
Materials and Structures

DISSIPATION ENERGY AS A STIMULUS FOR CORTICAL BONE ADAPTATION

Natarajan Chennimalai Kumar, Iwona Jasiuk and Jonathan Dantzig

msp

DISSIPATION ENERGY AS A STIMULUS FOR CORTICAL BONE ADAPTATION

Natarajan Chennimalai Kumar, Iwona Jasiuk and Jonathan Dantzig

We present a finite element study of a poroelastic rectangular beam subjected to oscillatory bending loads. This geometric model is chosen for simplicity, as an idealized representation of cortical bone. We then propose the use of the dissipation energy of the poroelastic flow as a mechanical stimulus for bone adaptation, and show that it can predict the effect of frequency of the applied load. Surface adaptation in the model depends on the weighted average of the mechanical stimulus in a "zone of influence" near each surface point, in order to incorporate the non-locality in the mechanotransduction of osteocytes present in the lacunae. We show that the dissipation energy stimulus and the resulting increase in second moment of inertia of the cross section increase linearly with frequency in the low frequency range (less than 10 Hz) and saturate at the higher frequency range (greater than 10 Hz). Similar non-linear adaptation frequency response also has been observed in numerous experiments. Our framework is readily extended to the modeling of cortical bone using actual bone geometries.

1. Introduction

Bone is a mechanically sensitive biological tissue, which adapts its size, shape, mass and density based on its mechanical environment [Cowin 2001]. It has been long recognized that a dynamic stimulus is required for bone adaptation [Rubin and Lanyon 1984; Turner 1998; Lanyon and Rubin 1984]. Researchers have shown that the adaptation depends on a combination of different mechanical stimuli such as the magnitude [Rubin and Lanyon 1984; Burr et al. 2002; Lanyon et al. 1982] and frequency of applied load [Burr et al. 2002; Lanyon et al. 1982; Hsieh and Turner 2001; Warden and Turner 2004], number of cycles [Rubin and Lanyon 1984; Turner 1998], and bouts of the applied loading [Robling et al. 2000; Robling et al. 2001; 2002]. The adaptation response is initiated when the applied strain exceeds a threshold value, and increases with the magnitude of applied strain [Rubin and Lanyon 1984; Lanyon et al. 1982]. Turner et al. [1994] observed significant cortical bone adaptation when the loading frequency exceeded 0.5 Hz. At low frequencies (between 0.5 and 10 Hz), it has been observed that adaptation in rat ulnae follows an approximately linear dose-response relationship with frequency [Hsieh and Turner 2001]. Warden and Turner [2004] found no significant increase in the adaptation response when the frequency of loading was increased beyond 10 Hz. Rubin and coworkers investigated the effect of very low magnitude high frequency (greater than 30 Hz) loading on sheep standing on a vibrating plate 20 minutes per day for a year. Trabecular bone volume increased more than 30%, but no significant changes were found in the cortical bone [Rubin et al. 2001; 2002]. Qin et al. [2001; 2000; 1999] showed that cortical bone responds to applied pressure gradients in the intermedullary fluid through periosteal bone formation, without any applied mechanical loading.

Several groups have examined the relationship between mechanical loading on bone and the associated fluid flow inside the various internal porosities. Knothe Tate and Knothe observed the fluid flow in and out of cortical bone in sheep forearms under applied load [Knothe Tate and Knothe 2000]. Knothe Tate et al. showed similar load-induced fluid flow in rat tibia subjected to bending, and also indicated the role of the fluid flow in mechanotransduction [Knothe Tate et al. 2000]. Numerous mechanisms have been proposed to explain the effect of fluid flow on the osteocytes e.g., via shear stress on the cell surface [Reich et al. 1990], drag force on the transverse fibrils that tether the osteocyte to the canalicular walls [Weinbaum et al. 1994], strain generated electric potentials [Pollack et al. 1984; Salzstein and Pollack 1987], or biochemical diffusive gradients [Robling et al. 2008].

Weinbaum and co-workers developed an analytical model that describes the hierarchical nature of the lacunocanalicular porosity in the cortical bone, using the results from Zhang and Cowin [Zhang and Cowin 1994] at the macroscale, coupled to mechanical model at the cellular length-scale [Zhang and Cowin 1994; You et al. 2001; Han et al. 2004]. These works demonstrated that the fluid-induced shear stress and drag force on the osteocyte process tethering fibers can amplify local strains by more than 50 times compared to the tissue level strains [Han et al. 2004]. They also showed that the strain amplification factor varies non-linearly with respect to the loading frequency, in a similar way as the adaptation response observed in the experiments mentioned earlier. Fritton and Weinbaum's extensive review [2009] provides a more complete description of fluid flow induced mechanotransduction in cortical bone.

In [Chennimalai Kumar et al. 2010] we developed a framework for modeling cortical bone adaptation which included: elastic finite element (FE) analysis of loading applied to geometrically accurate models of bone, extraction of a mechanical stimulus from the FE results to be used in an adaptation law, and simulation of adaptation by direct modification of the FE model. The adaptation procedure is implemented in a generic way so that it can be used to simulate the effect of the different mechanical loading parameters such as magnitude, frequency, number of bouts of loading, time between bouts, and other factors. We showed that an elastic material model and a simple growth law using strain energy density as the mechanical stimulus could predict the effect of load magnitude and the number of bouts of loading on adaptation of rat ulnae [Chennimalai Kumar et al. 2010]. In this paper, we extend that work to incorporate poroelastic analysis. Previous works have included poroelasticity in the adaptation equation, using the fluid shear stress and octahedral strain to compute the tissue phenotype for fracture [Lacroix and Prendergast 2002; Prendergast et al. 1997]. We propose a new mechanical stimulus based on the viscous dissipation energy due to the fluid flow as the stimulus for adaptation. We show that this stimulus can simulate the dependence of adaptation on loading frequency similar to the adaptation response observed experimentally. We consider the idealized bone geometry in the shape of a rectangular beam (following [Zhang and Cowin 1994]). This allows us to focus on the frequency trends by conducting a parametric study with relatively small computational resources.

The paper is organized as follows: We begin with a brief description of the theory of poroelasticity as it applies to bone, and identify a problem with an analytical solution to test our formulation. We then develop a measure of the mechanical stimulus to be used in an adaptation law. The results of simulations performed for a range of frequencies are presented, and these results are then interpreted in the context of mechanotransduction.

2. Theory of poroelasticity

Cortical bone is a porous structure with different porosities at different length scales [Cowin 1999], the most important being:

Vascular porosity: which is comprised of the cylindrical pathways of blood flow in the Haversian and Volkmann canals that form the osteonal structure of the cortical bone. The fluid permeability at this scale is of the order of 10^{-12} m^2 [Zhang et al. 1998a]. This porosity plays an important role in adaptation by delivering nutrients to the cells that form or resorb bone. Since the blood flow is from the vascular system, the pressure of the fluid in the vascular porosity is of the order of the physiological blood pressure.

Lacunocanalicular porosity: consisting of the porous regions of the lacunae surrounding the center of the osteon and the interconnecting canaliculi. The stimuli-sensing osteocyte cells reside within the pores of the lacunae and their processes are housed in the canaliculi. Zhang et al. [1998b] estimated permeability at this scale of porosity to be $10^{-18} - 10^{-21}$ m^2.

Collagen-apatite porosity: is seen at the nanostructural scale. This porosity contains water which is considered to be part of bone's collagen-apatite nanostructure. The flow of water through the pores between the organic collagen and the apatite mineral can be neglected [Cowin 2001].

It has been shown in a number of experimental and analytical works that the mechanical loading acting on bone induces the flow of fluid in and out of these different porosities [Knothe Tate 2001]. Weinbaum and co-workers showed the importance of the lacunocanalicular porosity for mechanotransduction in bone, where they hypothesize that osteocytes are deformed through the viscous shear stress due to the fluid flow inside the canaliculi [Weinbaum et al. 1994; You et al. 2001; Han et al. 2004]. These studies motivate the use of a poroelastic material model for the cortical bone with lacunocanalicular porosity.

We provide here a short overview of the theory of poroelasticity to establish the context for the poroelastic analyses presented in this paper, and refer the interested reader to more comprehensive treatments in the literature, such as [Biot 1941; Biot and Willis 1957; Coussy 1995; Detournay and Cheng 1993]. A poroelastic medium is made up of a solid matrix and pores. We consider saturated media, in which all of the pores are filled with fluid. There are four field variables: stress tensor $\boldsymbol{\sigma}$, strain tensor $\boldsymbol{\epsilon}$, pore pressure p, and the variation in fluid content ζ. The medium is characterized by its porosity n_p, the bulk modulus of the solid K_s, shear modulus of the solid G, Poisson's ratio for the solid ν, and the bulk modulus of the fluid K_f. The constitutive equations for an isotropic linear poroelastic material are

$$2G\epsilon_{ij} = \sigma_{ij} - \left(\frac{\nu}{\nu+1}\right)\sigma_{kk}\delta_{ij} + \alpha\left(\frac{1-2\nu}{1+\nu}\right)p\delta_{ij}, \quad 2G\zeta = \alpha\left(\frac{1-2\nu}{1+\nu}\right)\left(\sigma_{kk} + \frac{3p}{B}\right),$$

where we have introduced two additional parameters: the Willis coefficient α, and Skempton's coefficient B. The Willis coefficient can be thought of as the ratio of fluid volume gained (or lost) in a poroelastic element due to volume change when loaded under drained condition ($p = 0$). It can be shown that $\alpha = 1 - K/K_s$, where K is the drained bulk modulus. Similarly, Skempton's coefficient B is obtained from the undrained condition ($\zeta = 0$) as $p = -B\sigma_{kk}/3$.

The fluid flow rate is computed from the pressure using Darcy's law,

$$q_i = -\kappa\frac{\partial p}{\partial x_i} \tag{1}$$
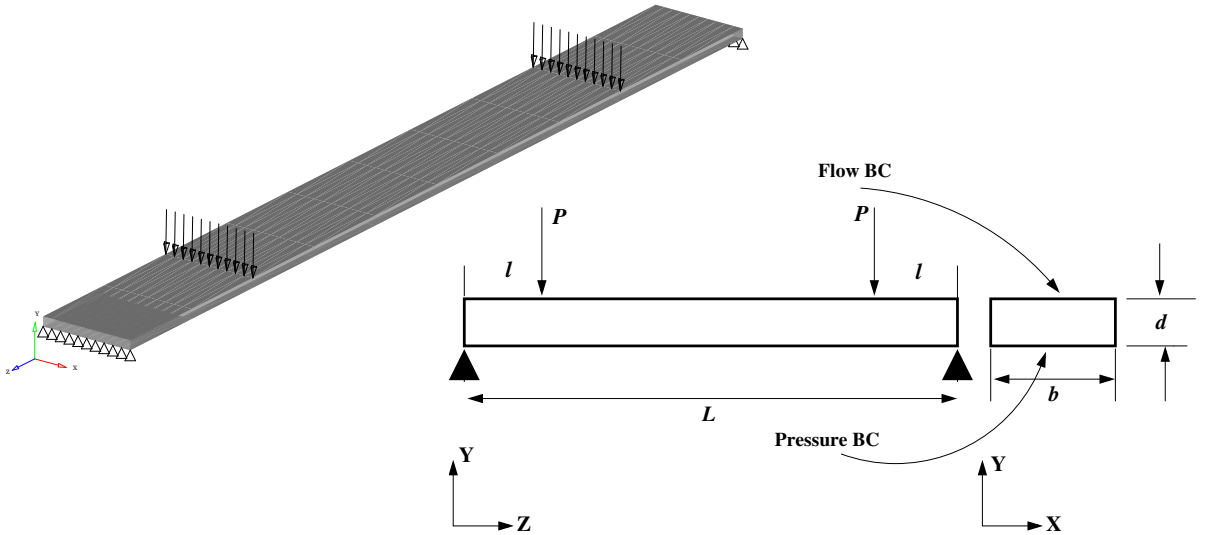
Figure 1. Schematic of the four-point bending setup of the rectangular poroelastic beam: isometric view (top left) and orthographic view with boundary conditions.

where the subscript i represents the coordinate direction, and q_i is the fluid mass flow rate and κ is the hydraulic permeability ($\kappa = k/\mu$, where k is the isotropic intrinsic permeability with units of m^2 and μ is the dynamic viscosity of the fluid). The fluid mass flow rate q_i is related to the fluid flow velocity v_i^{fl} as $q_i = n_p v_i^{\text{fl}}$, where ρ_{fl} is the density of the fluid.

Inserting the constitutive equations and Darcy's law into the mass and momentum balance equations leads to the following equation for the pore pressure:

$$c\nabla^2\left(\sigma_{kk} + \frac{3}{B}p\right) = \frac{\partial}{\partial t}\left(\sigma_{kk} + \frac{3}{B}p\right) \tag{2}$$

where c is the hydraulic diffusivity, defined as

$$c = \frac{2GB^2\kappa(1-\nu)(1+\nu_u)^2}{9(1-\nu_u)(\nu_u-\nu)} \tag{3}$$

where ν_u is the undrained Poisson's ratio. Scaling the length in all directions by a characteristic length d (that is, $X^* = x/d$), and scaling time using the frequency $\omega(T^* = \omega t)$, Equation (2) becomes

$$c\nabla^{*^2}\left(\sigma_{kk} + \frac{3}{B}p\right) = \text{Fo}\frac{\partial}{\partial T^*}\left(\sigma_{kk} + \frac{3}{B}p\right), \tag{4}$$

where $\text{Fo} = \omega d^2/c$ is the Fourier number, which represents the ratio of the timescale for hydraulic diffusion (d^2/c) to the timescale of the applied load ($1/\omega$). For small Fourier number ($\text{Fo} \ll 1$), the transient term on the right hand side can be neglected in comparison to the left hand side, and the pressure solution will be essentially quasi-static. For large values of Fourier number ($\text{Fo} \gg 1$), the Laplacian on the left hand side of the equation can be neglected and the pore pressure follows the stress solution. When Fo is of order one, the two sides balance. This observation will help us explain the results of our simulations.

The objective of this paper is to establish a frequency-dependent mechanical stimulus. To this end, we use as a test problem the bending of a poroelastic rectangular beam, similar to that considered in [Zhang and Cowin 1994]. Since our eventual goal is to analyze geometrically accurate bone models, we solve this problem using the finite element (FE) method, as implemented in the commercial software ABAQUS [2008]. We consider a beam of length L, width b, and thickness d, subjected to a cyclic 4-point bending load of the form $P = P_0/2(1 - \cos \omega t)$. The geometry and boundary conditions (BC) are illustrated in Figure 1. In order to simulate the BCs of a 4-point beam bending, we set $u_y = 0$ at both ends of the beam, and constrain one point, such that $u_x = 0$ and $u_z = 0$ as well to avoid rigid body motion. The bending loads are at a distance l from each end of the beam, as shown. The periosteal (outer) surface of a long bone is highly impermeable and the endosteal (inner) surface is highly permeable [Steck et al. 2003]. To simulate these properties in our model, we apply a zero pressure BC on the bottom surface, and zero flow BC on the top surface. We note that the latter BC is actually implemented via Darcy's law (1) as $\nabla p \cdot \boldsymbol{n} = 0$, where $\boldsymbol{n}$ is the normal vector.

3. Development of the stimulus for the growth law

The general form of the growth law used to model the bone adaptation is

$$\frac{\mathrm{d}b}{\mathrm{d}T} = A(\phi - \phi_{\mathrm{ref}}) \tag{5}$$

where b is a material characteristic (such as density, mass or shape), T is the growth timescale, A is a proportionality constant which we refer to as "gain", ϕ is a mechanical stimulus, and ϕ_{ref} is the reference stimulus that must be exceeded to trigger bone growth. Different types of growth stimuli have been proposed in the literature, such as strain energy density [Weinans et al. 1992; Huiskes et al. 2000], strain [Cowin and Hegedus 1976], daily stress [Carter et al. 1989; Carter et al. 1996], and others. In [Chenni-malai Kumar et al. 2010] we used the strain energy density as the mechanical stimulus to numerically model the bone growth response in a rat ulna using the growth algorithm shown in Figure 2. We describe the approach here briefly.
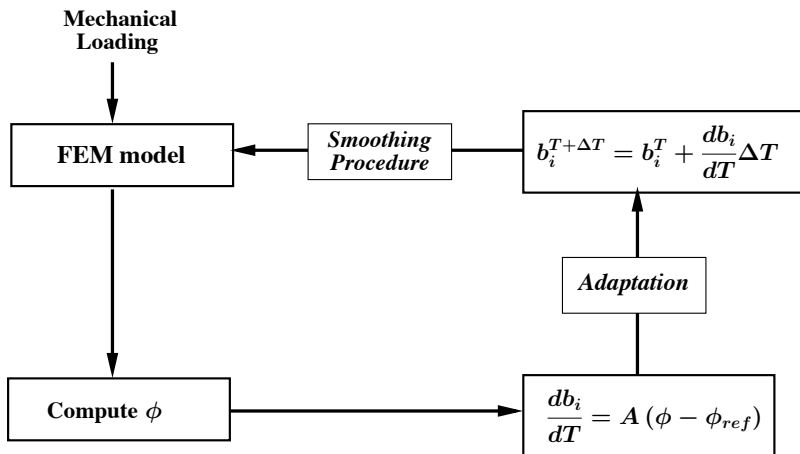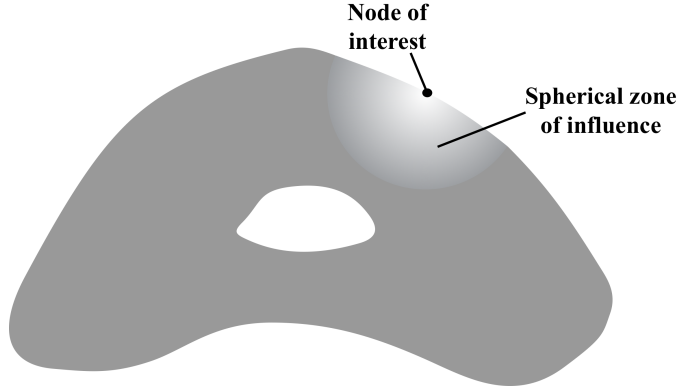

Figure 2. Flowchart describing the implementation of the adaptation procedure.

Figure 3. Schematic of the spherical zone of influence on a typical bone cross section. The shading is intended to show the decreasing influence of stimulus with distance from the surface node.

The FE model of the bone is created from micro-CT images, and a set of nodes on the outermost surface are identified as movable. An elastic analysis is carried out to compute the stresses and strains in the bone under an applied load. The strain energy densities in each finite element, including all surface nodes, are determined, and the displacement of a surface node is calculated based on the growth law

$$\frac{\mathrm{d}b_i}{\mathrm{d}T} = \begin{cases} A(\phi_i - \phi_{\text{ref}}) & \text{if } \phi_i \geq \phi_{\text{ref}}, \\ 0 & \text{if } \phi_i < \phi_{\text{ref}}. \end{cases} \tag{6}$$

where b_i is the displacement of the surface node i and ϕ_i is the local strain energy density at node i. Resorption was not observed in the experiments that were simulated [Robling et al. 2002], so we precluded resorption in our model. Note that the growth-timescale T is much longer than the timescale of loading (t in the poroelastic field equations). Once the rates of change of the position of the surface nodes are computed, the new positions of the nodes are computed using a forward Euler scheme for (6), followed by application of a smoothing filter. See [Chennimalai Kumar et al. 2010] for details. The new FE model is then constructed and the procedure is repeated. We were able to find significant agreement between the model and experiments using the strain energy density stimulus, for an elastic material model and quasi-static loading. However, the strain energy density cannot simulate the effect of loading frequency. Our goal in this work is to develop a stimulus similar to the strain energy density that is dependent on frequency.

We would like to have a stimulus that captures the fluid flow in the bone, and reduces it to a convenient scalar quantity. To that end, we choose the dissipation due to the viscous fluid flow [Coussy 1995], defined as

$$\phi = -n_p \boldsymbol{v}^{\text{fl}} \cdot \nabla p = \tfrac{1}{2}\left(n_p \boldsymbol{v}^{\text{fl}}\right) \cdot \boldsymbol{\kappa}^{-1} \cdot \left(n_p \boldsymbol{v}^{\text{fl}}\right) \tag{7}$$

where $\boldsymbol{v}^{\text{fl}}$ is the fluid velocity vector, ∇p is the pressure gradient, and $\boldsymbol{\kappa}$ is the hydraulic permeability tensor. We choose this form because it has been shown in a number of experiments, and hypothesized in analytical models, that the shear stress exerted by the fluid flow on the osteocyte cells is a possible candidate for mechanotransduction. Note that in the work that follows, we will take $\boldsymbol{\kappa}$ to be isotropic.

Osteocytes are interconnected through the processes inside the canalicular space. We hypothesize that they can communicate with each other through these processes and exchange information on the current state of the stimulus at each location. To simulate this non-local behavior, we propose the use of a spatially averaged stimulus over a "zone of influence" (ZOI), shown schematically in Figure 3. For the sake of simplicity, we choose a spherical zone of influence of radius r. The stimulus that triggers the growth response at a surface node i is then defined as

$$\phi_i = \frac{\int_V \left(\int_0^T \frac{1}{2} n_p \boldsymbol{v}^{\text{fl}} \cdot \kappa^{-1} \cdot n_p \boldsymbol{v}^{\text{fl}} \, dt \right) f(|\boldsymbol{x}|) \, dV}{\int_V f(|\boldsymbol{x}|) \, dV} \tag{8}$$

where $f(|\boldsymbol{x}|)$ is a function that weights the dissipation potential at an inner node by its distance $|\boldsymbol{x}|$ from the surface node i, and V is the volume of the zone of influence. Mullender et al. [1994] introduced a similar zone of influence in a study of internal remodeling, in which they used the strain energy in the neighborhood of each point, weighted by an exponential function, as the stimulus for remodeling. In the results presented below, we chose the form, $f(|\boldsymbol{x}|) = \exp(-5|\boldsymbol{x}|/d)$, where d is the thickness of the beam. The factor five was selected to ensure that any spurious high velocities at the inner surface, resulting from the boundary condition, do not affect the response. Numerical experiments showed that the results were not very sensitive to this factor, as long as it was larger than five.

4. Simulation details

The various material parameters used in the rectangular beam simulations, tabulated in Table 1, were chosen to be similar to properties of rat bone. The material properties given in the table are similar to those used in [Zhang and Cowin 1994]. The permeability of the lacunocanalicular porosity is reported to be in the range of 10^{-18} to 10^{-21} m² [Weinbaum et al. 1994; Salzstein and Pollack 1987]. Permeability will be shown to be a very important parameter in this problem, which directly affects the timescale of fluid diffusion in the poroelastic medium. The value of permeability we chose results in a significant range of Fourier numbers (from 12 to 380) for the physiological range of frequencies (1 Hz to 30 Hz). The hydraulic diffusivity corresponding to the permeability given in Table 1 is $c = 0.5606$ mm²/s. One can then estimate the characteristic time for hydraulic diffusion in a 1 mm thick beam to be of the order of one second.

Property	Value	Units
Young's modulus of bone E	12.0	GPa
Fluid bulk modulus K_f	2.3	GPa
Solid bulk modulus K_s	17.0	GPa
Porosity n_p	0.05	–
Drained Poisson's ratio ν	0.3	–
Intrinsic permeability k	3×10^{-20}	m²

**Table 1.** Values of different poroelastic parameters used in the analysis.
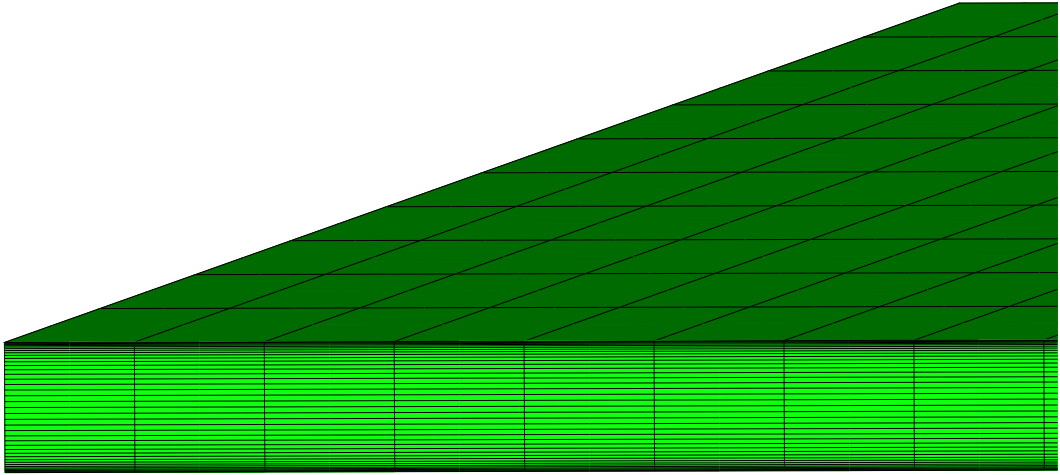
Figure 4. Finite element mesh of the rectangular beam. Note the biased mesh across the cross-section.

The FE mesh for our analyses, shown in Figure 4, consists of 18,821 nodes and 4000 triquadratic hexahedral elements. The elements are graded along the y-axis in order to accurately enforce the zero-flow boundary condition. A grid convergence study showed that this grid resulted in velocities of the order 10^{-4} mm/s on the top surface, which when compared to velocities in the bulk (of the order of 1 mm/s) were judged to be sufficiently small. The poroelastic solver in ABAQUS [2008] uses an unconditionally stable backward Euler integration scheme to solve (2). The accuracy of the solution still depends on the size of the timestep. We performed a convergence study to establish the timestep size as well, and we found that accurate results were obtained for $\Delta t < 0.5 h^2/c$, where h is the characteristic length of the smallest element. For the grid and properties used in the simulations reported below, this criterion gives $\Delta t = 5 \times 10^{-4}$ s. The applied load P_0 was chosen as 100 N.

5. Results

Figure 5 shows the time evolution of pore pressure and the fluid velocity at different points in the rectangular cross section for several different frequencies. In each case, there is an initial transient in both the pore pressure and fluid velocity that dies out after about 0.5 sec, which is of the order of the timescale of hydraulic diffusion noted earlier. After this time, pore pressure and velocity at each point follow a sinusoidal profile with the same frequency as the applied load. This is important, because it allows us to extrapolate the pore pressure and velocity solutions at the end of the initial transient to the entire duration of the experiments, which may be several minutes [Warden and Turner 2004], thus reducing the computational cost significantly. The velocities are maximal at the bottom surface, falling to zero at the top. Note that both the pore pressure at the upper surface, and the velocity at the lower surface, are out of phase with their respective values at the neutral axis.

Figure 6 shows the pore pressure and velocity profiles through the thickness for frequencies at 1 Hz, 5 Hz and 30 Hz, at different times within a single load cycle after the initial transient. We denote the
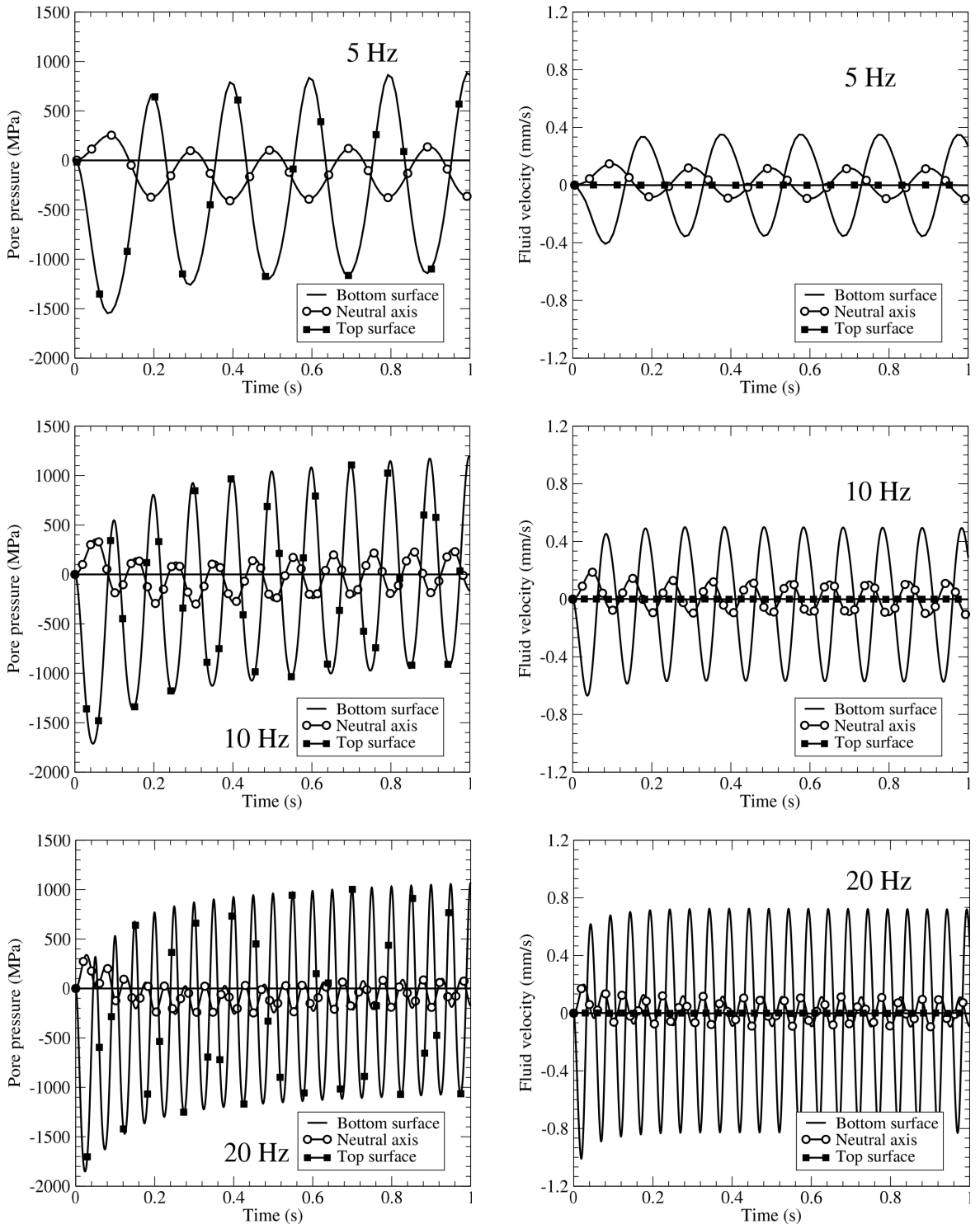
Figure 5. Plots of pore pressure (left column) and fluid flow velocity (right column) solutions as a function of time for three frequencies: 5 Hz, 10 Hz, and 20 Hz.
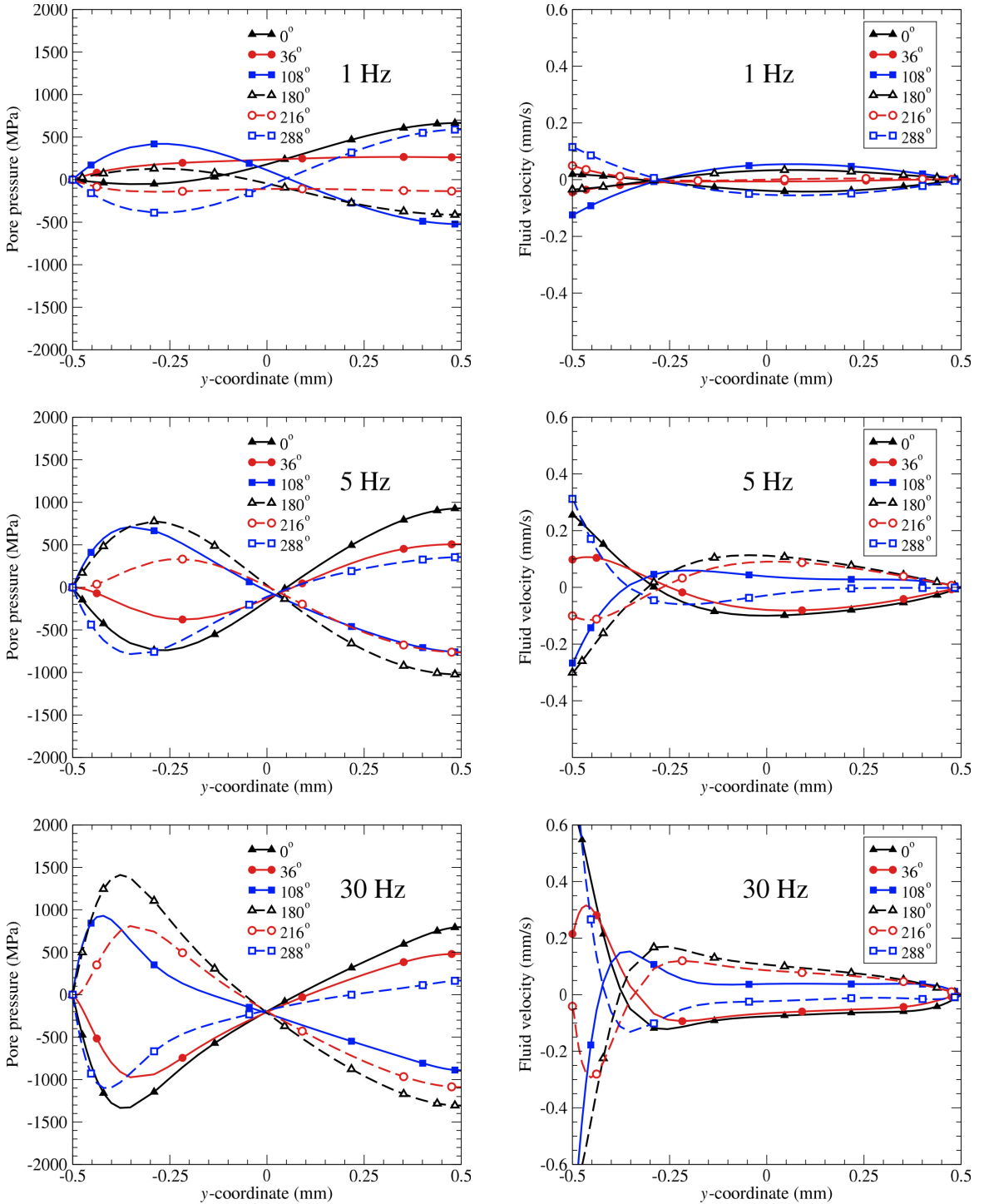
Figure 6. Plots of pore pressure (left column) and fluid flow velocity (right column) solutions across the cross-section at different points of time in a loading cycle (shown here as the phase angle) for three frequencies: 1 Hz, 5 Hz and 30 Hz.
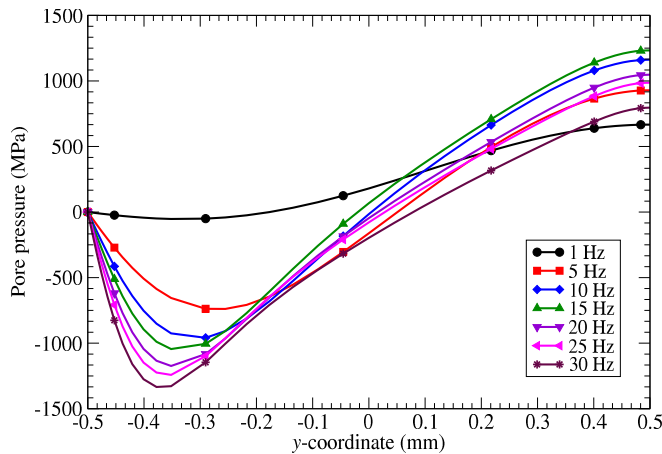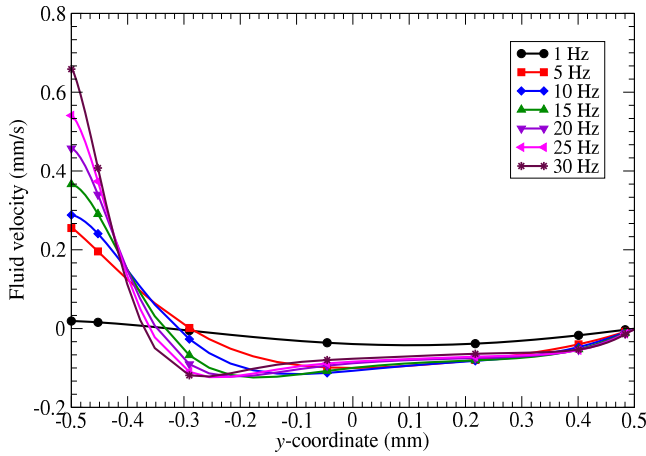
Figure 7. Plot of pore pressure solution across the cross-section for different frequencies at the end of a loading cycle.

various times within the cycle in degrees, where zero corresponds to the maximum in the load cycle. At 1 Hz (Figure 6, top left), the slope of the pore pressure distribution reaches zero midway between the bottom surface and the neutral axis, indicating zero flow velocity there. Figure 6, top right, which shows the corresponding fluid velocity, indicates that the velocity on the bottom surface is of a higher magnitude and has a smooth variation throughout the profile. The zero velocity solution is observed at the same location throughout the loading period.

At 5 Hz (Figure 6, middle), the pore pressure remains very close to zero at the neutral axis throughout the load cycle. The location of the zero-slope in the pressure solution (zero velocity by Darcy's law) varies with time of loading, and the velocity is nearly uniform over much of the beam cross-section above the neutral axis for parts of the load cycle. These effects are more pronounced at 30 Hz (Figure 6, bottom). There is very large variation in pore pressure near the bottom surface, which then falls to almost zero at the neutral axis. The velocity is also very large near the bottom surface, and then nearly uniform (and much smaller) over most of the remainder of the cross-section. Note that the computed velocities and pore pressures are considerably larger than those reported in [Rémond et al. 2008; Nguyen et al. 2010]. This is due to the application of a much larger load in our analysis. These quantities should be proportional to the magnitude of the applied load, because the problem is linear. We will address this issue in a future paper, in which we apply the current analysis to the deformation of a rat ulna.

The results of our calculations are summarized in Figures 7 and 8, which compare the pore pressure and fluid velocity through the thickness for different frequencies. As the frequency increases, the variation in pore pressure increases near the bottom surface, and becomes close to linear between $y = -0.3$ mm to $y = 0.3$ mm of the thickness. It should also be noted that the magnitude of pore pressure near the top surface (where the pressure gradient is zero) increases for frequencies from 1 to 10 Hz, but starts decreasing for frequencies greater than 10 Hz. Figure 8 shows that for frequencies less than 10 Hz, the flow is significant to about 50% of the thickness, i.e., up to the neutral axis, whereas at higher frequencies, even though the velocity at the bottom surface increases, the flow velocity becomes very small before reaching 25% of the thickness.

Figure 8. Plot of the fluid velocity pressure solution across the cross-section for different frequencies at the end of a loading cycle.

The dissipation energy, given by the time integral of the dissipation potential (7), was then computed from the solutions extrapolated to 100 s using the results at the end of the initial transient. Figure 9 shows that the dissipation energy in the beam follows a similar trend as the fluid velocity. The dissipation energy at the bottom surface increases with frequency. Since the bottom surface is farthest from the top surface, where significant adaptation occurs, we hypothesize that the effect of the dissipation energy at the bottom surface will be very small on the adaptation at the top. To implement this hypothesis in our analysis, we choose the exponential weighting function described earlier, and also shown in Figure 9.
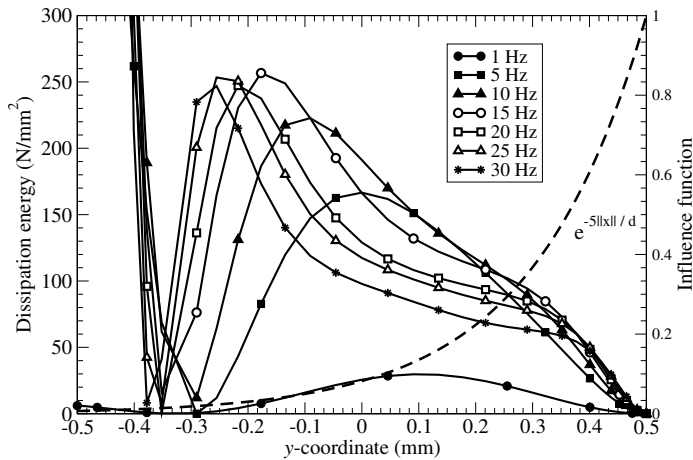
Figure 9. Plot of dissipation energy (time integral of dissipation potential) as a function of the y-coordinate for different frequencies. The influence function is also superimposed on the plot. We chose $\exp(-5\|x\|/d)$ as the influence function for our simulations. We have zoomed in on the plot to show the variation in the dissipation energy inside the beam, and so the very high values near $y = -0.5$ mm are cut off.
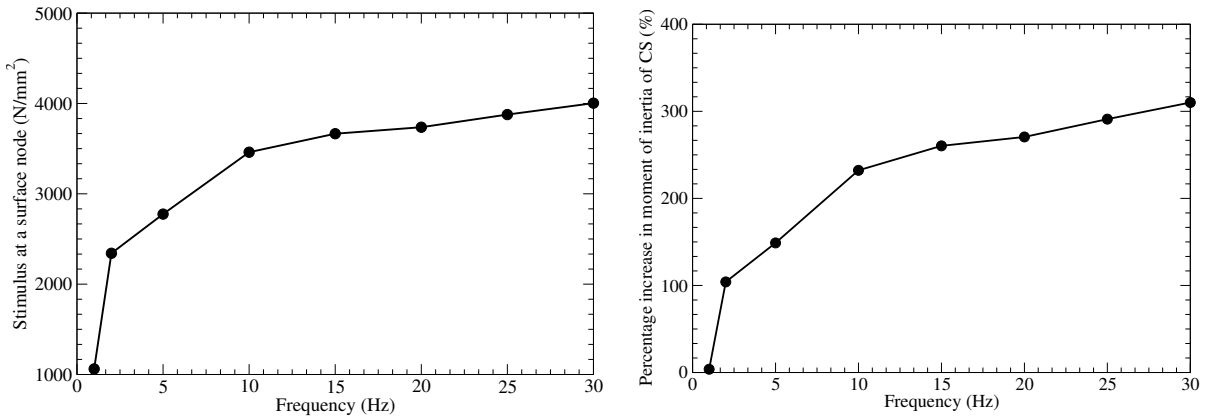
Figure 10. Left: plot of dissipation energy stimulus at a surface node as a function of loading frequency. Right: plot of percentage increase in the moment of inertia of the rectangular cross section due to adaptation as a function of frequency.

Figure 10, left, shows the adaptation stimulus (8) at a top surface node at the midspan of the beam as a function of the frequency of loading. We can see clearly that the adaptation stimulus increases rapidly at low frequencies, then saturates at about 10 Hz. We then used the growth law (6) to simulate growth of the rectangular beam for two growth timesteps, using a sensitivity $\phi_{\text{ref}} = 1000\,\text{N/mm}^2$ and a gain $A = 0.01\,\text{mm}^3/\text{N/timestep}$. We express the results as the percentage change in the moment of inertia of the rectangular cross section due to the adaptation. Figure 10, right, shows that the growth depends on frequency in a manner similar to the stimulus. This behavior is typical of that observed in numerous experiments; see [Burr et al. 2002; Lanyon et al. 1982; Hsieh and Turner 2001], and especially [Warden and Turner 2004].

6. Discussion

We have proposed the dissipation energy of the poroelastic flow induced by mechanical loading as the stimulus to trigger adaptation in cortical bone. We implemented this model using a rectangular beam because: (a) the geometry is simple and so the pressure and velocity solutions can be understood in greater detail; (b) and the problem has an analytical solution, which makes it easier to understand the role of the various physical parameters.

We found that at low frequencies, the flow first increases with loading frequency, but that as the frequency increases beyond 10 Hz, the amount of fluid that penetrates through the thickness of the beam decreases. This means that at the higher frequencies, there is less flow seen by the osteocytes in the lacunae, and hence they experience smaller shear and drag forces. The dissipation energy represents the work done by these forces, and thus at higher frequencies, the dissipation energy stimulus saturates, and hence one can expect the adaptation to saturate as well. Weinbaum and co-workers [Zhang and Cowin 1994; You et al. 2001; Han et al. 2004] analyzed the shear and drag forces on the osteocyte cell membrane due to the poroelastic flow at the cellular level, and showed that the amplification of the strains on the osteocyte cell membrane has a similar frequency response to our results for dissipation energy stimulus and increase in moment of inertia (Figure 10). The proposed dissipation energy stimulus that

we have put forth in this paper is thus qualitatively consistent with the strain amplification hypothesis and experimental observations.

We have also proposed the use of a "zone of influence" in order to simulate the effect of the distributed network of osteocytes and their communication. Osteocytes have been identified as the mechanosensory cells in the cortical bone. It has not yet been proven experimentally whether the osteocytes communicate with each other, and if so, what their mode of communication is. A series of experiments by Turner and coworkers on the expression of the sclerostin protein in response to *in vivo* mechanical loading suggest that there is such osteocyte communication, and also suggest the existence of a zone of influence. Robling et al. [2008] found that the expression of sclerostin protein, which is found almost exclusively in the osteocyte cells, is reduced considerably by *in vivo* mechanical loading, and further that the reduction in the sclerostin expression is much greater in the regions experiencing higher strains. The most pertinent observation for our work is that the expression of sclerostin is reduced on a group of osteocyte cells near the regions where higher bone growth is observed. This is a possible indication of the existence of a zone of influence within a real bone. Further experimental investigation of the expression of sclerostin at the scale of the osteocyte network could be used to inform the model as to the shape of the zone of influence.

7. Conclusions

We have performed poroelastic analyses on a simplified geometric model using the commercial FE software ABAQUS. We investigated the variations in pore pressure and fluid velocity with time and location in the beam, and their dependence on frequency. Based on these results, we propose the use of the dissipation energy as a mechanical stimulus for adaptation that can accommodate the effect of frequency. We also included the effect of non-locality of mechanotransduction of osteocytes present in the lacunae in the cortical bone through the use of a zone of influence. The dissipation energy stimulus evaluated in this manner is shown to increase linearly with frequency in the low frequency range, and saturate at the higher frequency range. The implementation of the poroelastic material model and the dissipation energy stimulus can be seamlessly integrated into our framework to simulate adaptation response on cortical bone. We are in the process of extending the poroelastic material model and the dissipation energy stimulus to the actual rat ulna FE model, and to quantitatively validate the numerical model with experimental observations.

Acknowledgments

References

[ABAQUS 2008] *ABAQUS Documentation*, Version 6.7, SIMULIA, Providence, RI, 2008, available at http://tinyurl.com/ABAQUS-docs-v6-7.

[Biot 1941] M. A. Biot, "General theory of three-dimensional consolidation", *J. Appl. Phys.* **12**:2 (1941), 155–164.

[Biot and Willis 1957] M. A. Biot and D. G. Willis, "The elastic coefficients of the theory of consolidation", *J. Appl. Mech. (ASME)* **24** (1957), 594–601.

[Burr et al. 2002] D. B. Burr, A. G. Robling, and C. H. Turner, "Effects of biomechanical stress on bones in animals", *Bone* **30**:5 (2002), 781–786.

[Carter et al. 1989] D. R. Carter, T. E. Orr, and D. P. Fyhrie, "Relationships between loading history and femoral cancellous bone architecture", *J. Biomech.* **22**:3 (1989), 231–244.

[Carter et al. 1996] D. R. Carter, M. C. H. van der Meulen, and G. S. Beaupré, "Mechanical factors in bone growth and development", *Bone* **18**:1, Supplement 1 (1996), S5–S10.

[Chennimalai Kumar et al. 2010] N. Chennimalai Kumar, J. A. Dantzig, I. M. Jasiuk, A. G. Robling, and C. H. Turner, "Numerical modeling of long bone adaptation due to mechanical loading: correlation with experiments", *Ann. Biomed. Eng.* **38**:3 (2010), 594–604.

[Coussy 1995] O. Coussy, *Mechanics of porous continua*, Wiley, Chichester, 1995.

[Cowin 1999] S. C. Cowin, "Bone poroelasticity", *J. Biomech.* **32**:3 (1999), 217–238.

[Cowin 2001] S. C. Cowin (editor), *Bone mechanics handbook*, 2nd ed., CRC Press, Boca Raton, FL, 2001.

[Cowin and Hegedus 1976] S. C. Cowin and D. H. Hegedus, "Bone remodeling, I: theory of adaptive elasticity", *J. Elasticity* **6**:3 (1976), 313–325.

[Detournay and Cheng 1993] E. Detournay and A. H.-D. Cheng, *Fundamentals of poroelasticity*, edited by C. Fairhurst, Pergamon, 1993.

[Fritton and Weinbaum 2009] S. P. Fritton and S. Weinbaum, "Fluid and solute transport in bone: flow-induced mechanotransduction", *Annu. Rev. Fluid Mech.* **41**:1 (2009), 347–374.

[Han et al. 2004] Y. Han, S. C. Cowin, M. B. Schaffler, and S. Weinbaum, "Mechanotransduction and strain amplification in osteocyte cell processes", *Proc. Nat. Acad. Sci. USA* **101**:47 (2004), 16689–16694.

[Hsieh and Turner 2001] Y.-F. Hsieh and C. H. Turner, "Effects of loading frequency on mechanically induced bone formation", *J. Bone Miner. Res.* **16**:5 (2001), 918–924.

[Huiskes et al. 2000] R. Huiskes, R. Ruimerman, G. H. van Lenthe, and J. D. Janssen, "Effects of mechanical forces on maintenance and adaptation of form in trabecular bone", *Nature* **405**:6787 (2000), 704–706.

[Knothe Tate 2001] M. L. Knothe Tate, "Interstitial fluid flow", pp. 22:1–22:29 in *Bone mechanics handbook*, 2nd ed., edited by S. C. Cowin, CRC Press, Boca Raton, FL, 2001.

[Knothe Tate and Knothe 2000] M. L. Knothe Tate and U. Knothe, "An ex vivo model to study transport processes and fluid flow in loaded bone", *J. Biomech.* **33**:2 (2000), 247–254.

[Knothe Tate et al. 2000] M. L. Knothe Tate, R. Steck, M. R. Forwood, and P. Niederer, "In vivo demonstration of load-induced fluid flow in the rat tibia and its potential implications for processes associated with functional adaptation", *J. Exp. Biol.* **203**:18 (2000), 2737–2745.

[Lacroix and Prendergast 2002] D. Lacroix and P. J. Prendergast, "A mechano-regulation model for tissue differentiation during fracture healing: analysis of gap size and loading", *J. Biomech.* **35**:9 (2002), 1163–1171.

[Lanyon and Rubin 1984] L. E. Lanyon and C. T. Rubin, "Static vs. dynamic loads as an influence on bone remodelling", *J. Biomech.* **17**:12 (1984), 897–905.

[Lanyon et al. 1982] L. E. Lanyon, A. E. Goodship, C. J. Pye, and J. H. MacFie, "Mechanically adaptive bone remodelling", *J. Biomech.* **15**:3 (1982), 141–154.

[Mullender et al. 1994] M. G. Mullender, R. Huiskes, and H. Weinans, "A physiological approach to the simulation of bone remodeling as a self-organizational control process", *J. Biomech.* **27**:11 (1994), 1389–1394.

[Nguyen et al. 2010] V.-H. Nguyen, T. Lemaire, and S. Naili, "Poroelastic behaviour of cortical bone under harmonic axial loading: a finite element study at the osteonal scale", *Med. Eng. Phys.* **32**:4 (2010), 384–390.

[Pollack et al. 1984] S. R. Pollack, N. Petrov, R. Salzstein, G. Brankov, and R. Blagoeva, "An anatomical model for streaming potentials in osteons", *J. Biomech.* **17**:8 (1984), 627–636.

[Prendergast et al. 1997] P. J. Prendergast, R. Huiskes, and K. Soballe, "Biophysical stimuli on cells during tissue differentiation at implant interfaces", *J. Biomech.* **30**:6 (1997), 539–548.

[Qin et al. 1999] Y.-X. Qin, K. J. McLeod, and C. T. Rubin, "Intramedullary pressure induced fluid flow in bone", pp. 490 in *Proceedings of the First Joint BMES/EMBS Conference: serving humanity, advancing technology* (Atlanta, GA, 1999), vol. 1, edited by S. M. Blanchard et al., IEEE, Piscataway, NJ, 1999.

[Qin et al. 2000] Y.-X. Qin, M. Cute, and C. T. Rubin, "Bone morphological adaptation induced by dynamic fluid flow in the absence of matrix strain", *Ann. Biomed. Eng.* **28**:SUPPL 1 (2000), 1–8.

[Qin et al. 2001] Y.-X. Qin, A. Saldanha, and T. Kaplan, "Oscillatory bone fluid flow and its role in initiating remodeling in the absence of matrix strain", pp. 51–52 in *2001 advances in bioengineering: presented at the 2001 ASME International Mechanical Engineering Congress and Exposition* (New York, 2001), edited by B. B. Lieber, BED **51**, ASME, New York, 2001. Paper # BED-23025.

[Reich et al. 1990] K. M. Reich, C. V. Gay, and J. A. Frangos, "Fluid shear stress as a mediator of osteoblast cyclic adenosine monophospate production", *J. Cell. Physiol.* **143**:1 (1990), 100–104.

[Rémond et al. 2008] A. Rémond, S. Naili, and T. Lemaire, "Interstitial fluid flow in the osteon with spatial gradients of mechanical properties: a finite element study", *Biomech. Model. Mechanobiol.* **7**:6 (2008), 487–495.

[Robling et al. 2000] A. G. Robling, D. B. Burr, and C. H. Turner, "Partitioning a daily mechanical stimulus into discrete loading bouts improves the osteogenic response to loading", *J. Bone Miner. Res.* **15**:8 (2000), 1596–1602.

[Robling et al. 2001] A. G. Robling, D. B. Burr, and C. H. Turner, "Recovery periods restore mechanosensitivity to dynamically loaded bone", *J. Exp. Biol.* **204**:19 (2001), 3389–3399.

[Robling et al. 2002] A. G. Robling, F. M. Hinant, D. B. Burr, and C. H. Turner, "Improved bone structure and strength after long-term mechanical loading is greatest if loading is separated into short bouts", *J. Bone Miner. Res.* **17**:8 (2002), 1545–1554.

[Robling et al. 2008] A. G. Robling, P. J. Niziolek, L. A. Baldridge, K. W. Condon, M. R. Allen, I. Alam, S. M. Mantila, J. Gluhak-Heinrich, T. M. Bellido, S. E. Harris, and C. H. Turner, "Mechanical stimulation of bone *in vivo* reduces osteocyte expression of Sost/sclerostin", *J. Biol. Chem.* **283**:9 (2008), 5866–5875.

[Rubin and Lanyon 1984] C. T. Rubin and L. E. Lanyon, "Regulation of bone formation by applied dynamic loads", *J. Bone Joint Surg. Am.* **66**:3 (1984), 397–402.

[Rubin et al. 2001] C. Rubin, A. S. Turner, S. Bain, C. Mallinckrodt, and K. McLeod, "Low mechanical signals strengthen long bones", *Nature* **412**:6847 (2001), 603–604.

[Rubin et al. 2002] C. Rubin, S. Judex, and M. Hadjiargyrou, "Skeletal adaptation to mechanical stimuli in the absence of formation or resorption of bone", *J. Musculoskelet. Neuronal Interact.* **2**:3 (2002), 264–267.

[Salzstein and Pollack 1987] R. A. Salzstein and S. R. Pollack, "Electromechanical potentials in cortical bone, II: experimental analysis", *J. Biomech.* **20**:3 (1987), 271–280.

[Steck et al. 2003] R. Steck, P. Niederer, and M. L. Knothe Tate, "A finite element analysis for the prediction of load-induced fluid flow and mechanochemical transduction in bone", *J. Theor. Biol.* **220**:2 (2003), 249–259.

[Turner 1998] C. H. Turner, "Three rules for bone adaptation to mechanical stimuli", *Bone* **23**:5 (1998), 399–407.

[Turner et al. 1994] C. H. Turner, M. R. Forwood, and M. W. Otter, "Mechanotransduction in bone: do bone cells act as sensors of fluid flow?", *FASEB J.* **8**:11 (1994), 875–878.

[Warden and Turner 2004] S. J. Warden and C. H. Turner, "Mechanotransduction in the cortical bone is most efficient at loading frequencies of 5–10 Hz", *Bone* **34**:2 (2004), 261–270.

[Weinans et al. 1992] H. Weinans, R. Huiskes, and H. J. Grootenboer, "The behavior of adaptive bone-remodeling simulation models", *J. Biomech.* **25**:12 (1992), 1425–1441.

[Weinbaum et al. 1994] S. Weinbaum, S. C. Cowin, and Y. Zeng, "A model for the excitation of osteocytes by mechanical loading-induced bone fluid shear stresses", *J. Biomech.* **27**:3 (1994), 339–360.

[You et al. 2001] L. You, S. C. Cowin, M. B. Schaffler, and S. Weinbaum, "A model for strain amplification in the actin cytoskeleton of osteocytes due to fluid drag on pericellular matrix", *J. Biomech.* **34**:11 (2001), 1375–1386.

[Zhang and Cowin 1994] D. Zhang and S. C. Cowin, "Oscillatory bending of a poroelastic beam", *J. Mech. Phys. Solids* **42**:10 (1994), 1575–1599.

[Zhang et al. 1998a] D. Zhang, S. Weinbaum, and S. C. Cowin, "Electrical signal transmission in a bone cell network: the influence of a discrete gap junction", *Ann. Biomed. Eng.* **26**:4 (1998), 644–659.

[Zhang et al. 1998b] D. Zhang, S. Weinbaum, and S. C. Cowin, "Estimates of the peak pressures in bone pore water", *J. Biomech. Eng.* (*ASME*) **120**:6 (1998), 697–703.

NATARAJAN CHENNIMALAI KUMAR: natarajan.uiuc@gmail.com
Department of Mechanical Science and Engineering, University of Illinois at Urbana-Champaign, 1206 West Green Street, Urbana, IL 61801, United States

IWONA JASIUK: ijasiuk@illinois.edu
Department of Mechanical Science and Engineering, University of Illinois at Urbana-Champaign, 1206 West Green Street, Urbana, IL 61801, United States
http://www.mechse.uiuc.edu/faculty/ijasiuk

JONATHAN DANTZIG: dantzig@illinois.edu
Department of Mechanical Science and Engineering, University of Illinois at Urbana-Champaign, 1206 West Green Street, Urbana, IL 61801, United States